fractal and fractional

MDPI

Article

Dynamic Analysis of a Novel 3D Chaotic System with Hidden and Coexisting Attractors: Offset Boosting, Synchronization, and Circuit Realization

Chengwei Dong

Department of Physics, North University of China, Taiyuan 030051, China; dongchengwei@tsinghua.org.cn

Abstract: To further understand the dynamical characteristics of chaotic systems with a hidden attractor and coexisting attractors, we investigated the fundamental dynamics of a novel three-dimensional (3D) chaotic system derived by adding a simple constant term to the Yang–Chen system, which includes the bifurcation diagram, Lyapunov exponents spectrum, and basin of attraction, under different parameters. In addition, an offset boosting control method is presented to the state variable, and a numerical simulation of the system is also presented. Furthermore, the unstable cycles embedded in the hidden chaotic attractors are extracted in detail, which shows the effectiveness of the variational method and 1D symbolic dynamics. Finally, the adaptive synchronization of the novel system is successfully designed, and a circuit simulation is implemented to illustrate the flexibility and validity of the numerical results. Theoretical analysis and simulation results indicate that the new system has complex dynamical properties and can be used to facilitate engineering applications.

Keywords: hidden attractor; coexisting attractors; offset boosting; symbolic dynamics; circuit simulation; adaptive synchronization

check for updates

Citation: Dong, C. Dynamic Analysis of a Novel 3D Chaotic System with Hidden and Coexisting Attractors: Offset Boosting, Synchronization, and Circuit Realization. *Fractal Fract.* **2022**, *6*, 547. https://doi.org/10.3390/fractalfract6100547

Academic Editor: Viorel-Puiu Paun

Received: 1 September 2022
Accepted: 22 September 2022
Published: 27 September 2022

1. Introduction

Since the meteorologist Lorenz discovered chaos phenomena in 1963 [1], chaos has been widely and deeply studied. As such, with the development of computer science and technology, several continuous chaotic systems have been discovered, including the Chua, Sprott, and Jerk systems [2–6]. The shapes of chaotic attractors are various, and the two representative shapes are the wing shape and scroll shape. Chaos widely exists in three-dimensional (3D) or high-dimensional continuous nonlinear dynamical systems. It is considerably important to produce new chaotic systems based on existing chaotic attractors when studying chaos. A wide range of engineering problems can be investigated by applying the complexity of chaotic systems [7], including image encryption, secure communication, and control and synchronization. Thus, it is of significance to analyze the dynamics of new chaotic systems.

Recent research involves classifying periodic and chaotic attractors as self-excited attractors or hidden attractors [8]. The self-excited attractor has an attraction basin associated with the unstable equilibrium, while the attraction basin of a hidden attractor does not intersect with the small neighborhood of any equilibria. It has been found that attractors in a dynamical system with stable equilibria [9–11], an infinite number of equilibria [12–17], or no equilibrium points [18–21] are hidden attractors. Owing to the unique dynamic characteristics of the hidden attractor, it has become a research hotspot in recent years. Self-excited and hidden chaotic attractors can be separately observed in Matouk's hyper-chaotic systems [22]. In Ref. [23], hidden attractors are put forward from an existing chaotic saddle through a boundary crisis. New 3D autonomous chaotic systems without linear terms, which have an infinite number of equilibrium points that display complex dynamics, have also been proposed [24,25]. In Ref. [26], a new inductor-free two-memristor-based chaotic circuit with three line equilibrium points was found. Synchronization and control of

a chaotic system with a hidden attractor has been implemented by numerical simulation [27]. Zeng et al. investigated a special memristor-based Jerk system in which self-excited and hidden attractors can be introduced [28]. Based on the Jerk chaotic system, a multi-scroll hyperchaotic system with hidden attractors that can produce any number of scrolls was also devised [29].

Many nonlinear dynamical systems often exhibit coexisting attractors in their respective attraction basins [30,31], and it is thus of great significance to discuss coexisting attractors. In Ref. [32], a new 4D chaotic system with coexisting and hidden attractors was generated. A novel 5D system with extreme multi-stability and hidden chaotic attractors has been presented [33]. Coexisting hidden attractors were also constructed in a 4D segmented disc dynamo [34]. In Ref. [35], coexisting hidden attractors with complex transient transition behaviors were explored in a simple 4D system with only one control parameter. The dynamics of a novel 4D multistable chaotic system having a plane as the equilibria has been introduced [36], and several interesting dynamic characteristics, such as antimonotone bifurcations and offset boosting, are also revealed via common nonlinear analysis tools. In Ref. [37], a new 5D chaotic system with a hidden attractor and coexisting attractors was derived and its dynamical behavior analyzed numerically. Pham et al. also discovered coexisting attractors in a novel 3D system without equilibria [38].

In this work, we constructed a novel 3D system with a double-wing chaotic attractor and two stable equilibrium points. The prominent feature of the new system is that it belongs to the category of hidden attractors. We also illustrated that the system is variable-boostable and has various coexisting attractors for a determined range of parameters. To the best of our knowledge, this combination of novel characteristics has not yet been reported in such a hidden attractor chaotic system with stable equilibrium points. Finally, we established an electronic analog circuit of the new double-wing chaotic system through MultiSIM, demonstrating that the mathematical model has practical feasibility for circuit realization.

This rest of this paper is organized as follows. Section 2 presents the mathematical model of the system and its dynamic characteristics. In Section 3, the complex dynamical behaviors of the new double-wing chaotic system are analyzed numerically, and basins of attraction of various coexisting attractors are shown. To systematically locate the unstable cycles embedded in the hidden chaotic attractor, 1D symbolic dynamics is introduced in Section 4, which can be reliably utilized in calculations. Section 5 presents the MultiSIM electronic circuit simulation study. To stimulate interest in such systems and realize robust technological applications, Section 6 introduces adaptive synchronization with unknown parameters. Finally, several concluding remarks are given in Section 7.

2. Mathematical Model and Its Properties

Yang and Chen proposed a new 3D chaotic system with one saddle and two stable node-focus points [39] that connects the Lorenz and Chen systems and denotes a transition from one to the other. The form of the Yang–Chen system is given in Equation (1), and the complex dynamics and compound structure of the system were investigated and discussed with careful numerical simulations [39]:

$$\begin{aligned} \frac{dx}{dt} &= a(y-x), \\ \frac{dy}{dt} &= cx - xz, \\ \frac{dz}{dt} &= xy - bz. \end{aligned} \tag{1}$$

Based on this system, we added a simple constant term to the third equation and obtained a novel 3D chaotic system,

$$\begin{aligned} \frac{dx}{dt} &= a(y-x), \\ \frac{dy}{dt} &= cx - xz, \\ \frac{dz}{dt} &= xy - bz - d, \end{aligned} \tag{2}$$

where a, b, c, and d are real parameters. Because Equation (2) is modified from Equation (1), and because Equation (1) is obtained from the classical Lorenz model without one dissipative term $-y$, the meanings of the parameters a, b, and c in Equation (2) should be the same as those in the classical Lorenz system, which are the Prandtl number, aspect ratio of the rolls, and Rayleigh number, respectively. d is chosen as a control parameter in order to observe the production of a hidden attractor in the system. When $a = c = 35$, $b = 3$, and $d = 0$, the system is the original Yang–Chen system. We take the values of parameters a, b, and c from the literature [39], and randomly take the newly introduced parameter d as 10. When $(a, b, c, d) = (35, 3, 35, 10)$ and the initial values are $(x_0, y_0, z_0) = (1, 1, 1)$, system (2) presents a strange attractor in the shape of a double wing, as shown in Figure 1. To further verify that system (2) is chaotic, the three Lyapunov exponents calculated by the Wolf algorithm [40] are expressed as follows:

$$LE_1 = 1.100, LE_2 = 0, LE_3 = -39.098.$$

The fractional dimension of the system can also be calculated, which indicates the complexity of the attractor. The Kaplan–Yorke dimension of system (2) is defined as follows:

$$D_{KY} = j + \frac{1}{|LE_{j+1}|} \sum_{i=1}^{j} LE_i,$$

where j denotes the largest integer satisfying $\sum_{i=1}^{j} LE_i \geq 0$ and $\sum_{i=1}^{j+1} LE_i < 0$. Therefore, the Kaplan–Yorke dimension for the parameters $(a, b, c, d) = (35, 3, 35, 10)$ is found to be

$$D_{KY} = 2 + (LE_1 + LE_2)/|LE_3| = 2.0281.$$

When the coordinates are transformed as $(x, y, z) \to (-x, -y, z)$, the form of system (2) remains unchanged, which implies that system (2) is rotationally symmetric about the z axis.

The fixed points of system (2) are determined by solving the following equation:

$$\begin{aligned} a(y-x) &= 0, \\ cx - xz &= 0, \\ xy - bz - d &= 0, \end{aligned} \tag{3}$$

and the two fixed points are then

$$\begin{aligned} &E_1 : (-\sqrt{bc+d}, -\sqrt{bc+d}, c), \\ &E_2 : (\sqrt{bc+d}, \sqrt{bc+d}, c). \end{aligned} \tag{4}$$

To analyze the stability of the two fixed points E_1 and E_2, we undertake the calculations for the Jacobian matrix of system (2):

$$J = \begin{pmatrix} -a & a & 0 \\ c-z & 0 & -x \\ y & x & -b \end{pmatrix}.$$

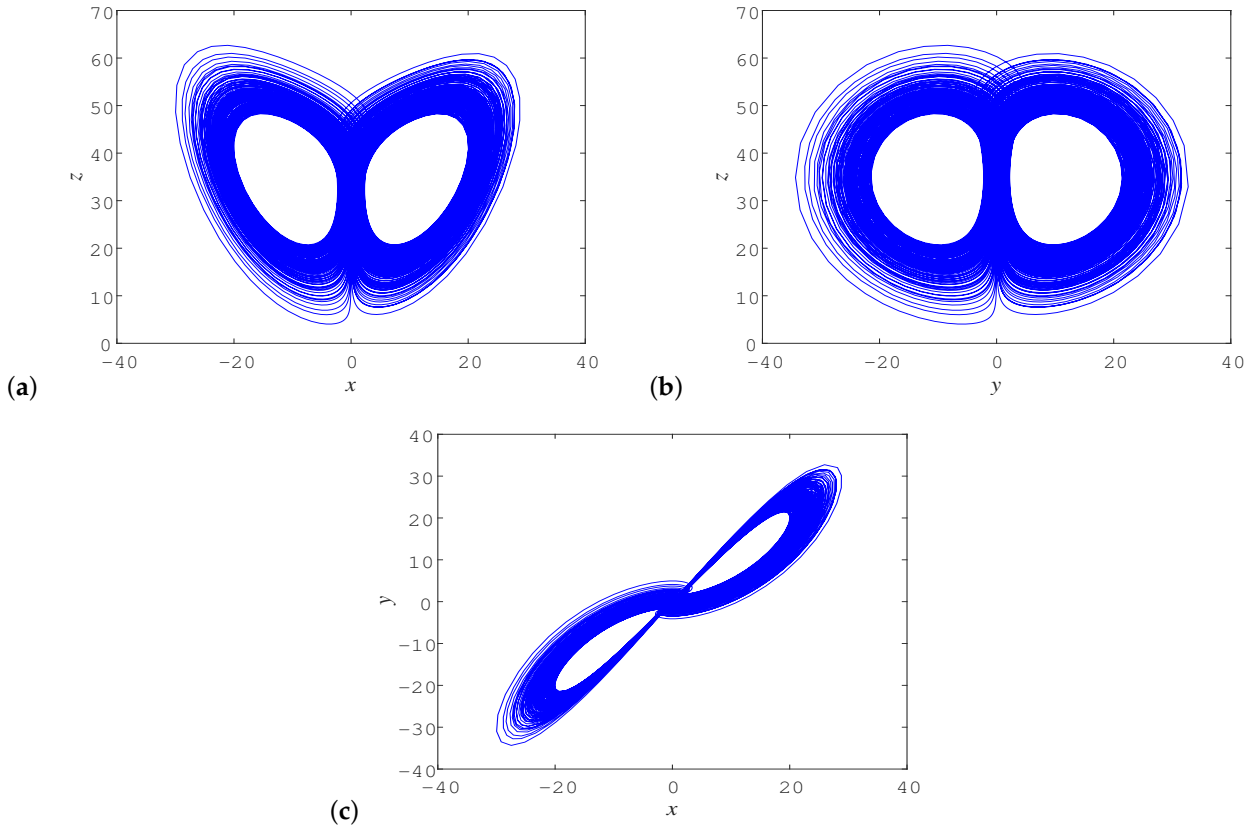

Figure 1. Two-dimensional projections of chaotic attractor onto various planes at time $t = 150$: (**a**) $x - z$, (**b**) $y - z$, and (**c**) $x - y$ planes.

We apply spectral stability theory to investigate the stabilities [41]. When the parameters are taken $(a, b, c, d) = (35, 3, 35, 10)$, the matrices $J(E_1)$ and $J(E_2)$ have the same spectral values $\lambda_1 = -37.812$, $\lambda_{2,3} = -0.094 \pm 14.591i$. Thus, the two fixed points are both stable node-focus points. System (2) possessing a chaotic attractor under current parameters means that the chaotic attractor is hidden.

The critical value of the Rayleigh parameter for a subcritical Hopf bifurcation that occurs in system (2) can also be obtained by using Routh–Hurwitz criterion. The characteristic equation is

$$f(\lambda) = \lambda^3 + (a + b)\lambda^2 + (ab - ac + x^2 + az)\lambda + ax^2 - abc + abz + axy.$$

By substituting the coordinates of the two fixed points in Equation (4) separately, we have the same characteristic equation:

$$f(\lambda) = a_3\lambda^3 + a_2\lambda^2 + a_1\lambda + a_0,$$

where

$$\begin{aligned} a_3 &= 1, \\ a_2 &= a + b, \\ a_1 &= ab + bc + d, \\ a_0 &= 2a(bc + d). \end{aligned}$$

From the Routh–Hurwitz criterion, the two fixed points E_1 and E_2 are stable if the following conditions are satisfied: $a_i > 0 (i = 0, 1, 2, 3)$ and $a_2a_1 - a_3a_0 > 0$. For the

parameters $(a, b, d) = (35, 3, 10)$, system (2) yields a critical value of 38.229 for the Rayleigh parameter c for a subcritical Hopf bifurcation.

The dissipativity of system (2) can be examined by calculating $\nabla \cdot V$, which gives

$$\nabla \cdot V = \frac{\partial \dot{x}}{\partial x} + \frac{\partial \dot{y}}{\partial y} + \frac{\partial \dot{z}}{\partial z} = -a - b.$$

Therefore, system (2) exhibits dissipativity when $-a - b < 0$, and volumes in phase space will shrink to 0 exponentially fast as $t \to \infty$.

For clarity, we compare the new system (2) and the chaotic system proposed previously by Dong [10], as listed in Table 1. Moreover, we also summarize the similarities and differences in analysis methods used in the two chaotic systems and tabulate them in Table 2, from which it can be seen that an implementation of a circuit will be applied in both studies.

Table 1. Comparison with two chaotic systems with initial values $(1, 1, 1)$.

Systems	Equations	Parameters	Equilibria	Eigenvalues	Lyapunov Exponents	Fractional Dimensions	Attractor Type
This work	$\dot{x} = a(y - x)$ $\dot{y} = cx - xz$ $\dot{z} = xy - bz - d$	$a = 35$ $b = 3$ $c = 35$ $d = 10$	$(-10.7238, -10.7238, 35)$ $(10.7238, 10.7238, 35)$	-37.812 $-0.094 \pm 14.591i$	1.100 0 -39.098	2.0281	Hidden
Dong [10]	$\dot{x} = a(y - x) + kxz$ $\dot{y} = -cy - xz$ $\dot{z} = -b + xy$	$a = 10$ $b = 100$ $c = 11.2$ $k = -0.2$	$(-11.0634, -9.0387, -9.1503)$ $(11.0634, 9.0387, -9.1503)$	-18.7413 $-0.314 \pm 11.424i$	0.7457 -0.0057 -26.8144	2.0276	Hidden
		$a = 10$ $b = 64$ $c = 0$ $k = 0$	$(-8, -8, 0)$ $(8, 8, 0)$	-12.8068 $1.4034 \pm 9.8983i$	1.4456 0.001 -11.4473	2.1264	Self-excited

Table 2. Analysis methods used in investigating the two chaotic systems.

	This Work	Dong [10]
Establishment of mathematical model	Adding a simple constant term $-d$ to Yang-Chen system	Adding a nonlinear term of cross-product kxz to generalized Lorenz-type system
Dynamics	Yes	Yes
Coexisting attractors	Yes	No
Offset boosting control	Yes	No
Symbolic dynamics of unstable cycles	Two letters	Four letters for hidden attractor Six letters for self-excited attractor
Circuit implementation	Yes	Yes
Synchronization	Yes	No

3. Dynamics of Novel Double-Wing Chaotic System

3.1. Bifurcation Diagram and Lyapunov Exponents

We investigated the dynamics of system (2) under different parameters by means of the bifurcation diagram with the Lyapunov exponents spectrum. The parameter region of interest is specified as $a \in [10, 60]$ and $b \in [0, 5]$, and the initial values are chosen as $(1, 1, 1)$. Taking the parameters a and b as variables, the remaining parameters of the system were fixed. By changing the parameters a and b, various states of system (2) can be observed.

The bifurcation diagram and corresponding Lyapunov exponents spectrum of system (2) by altering a are obtained in Figure 2a,b, respectively. It can be seen that system (2) exhibits chaotic and stable state behaviors versus different a values. Explicitly, system (2) exhibits chaotic behavior when $a < 40.5$, where one of the three Lyapunov exponents is greater than zero, one is equal to zero, and one is less than zero, whereas system (2) converges to a stable equilibrium point when $a \geq 40.5$, where the three Lyapunov exponents are all less than zero. In Figure 2c,d, the 3D projections of the phase portraits of system (2) in different states are also presented.

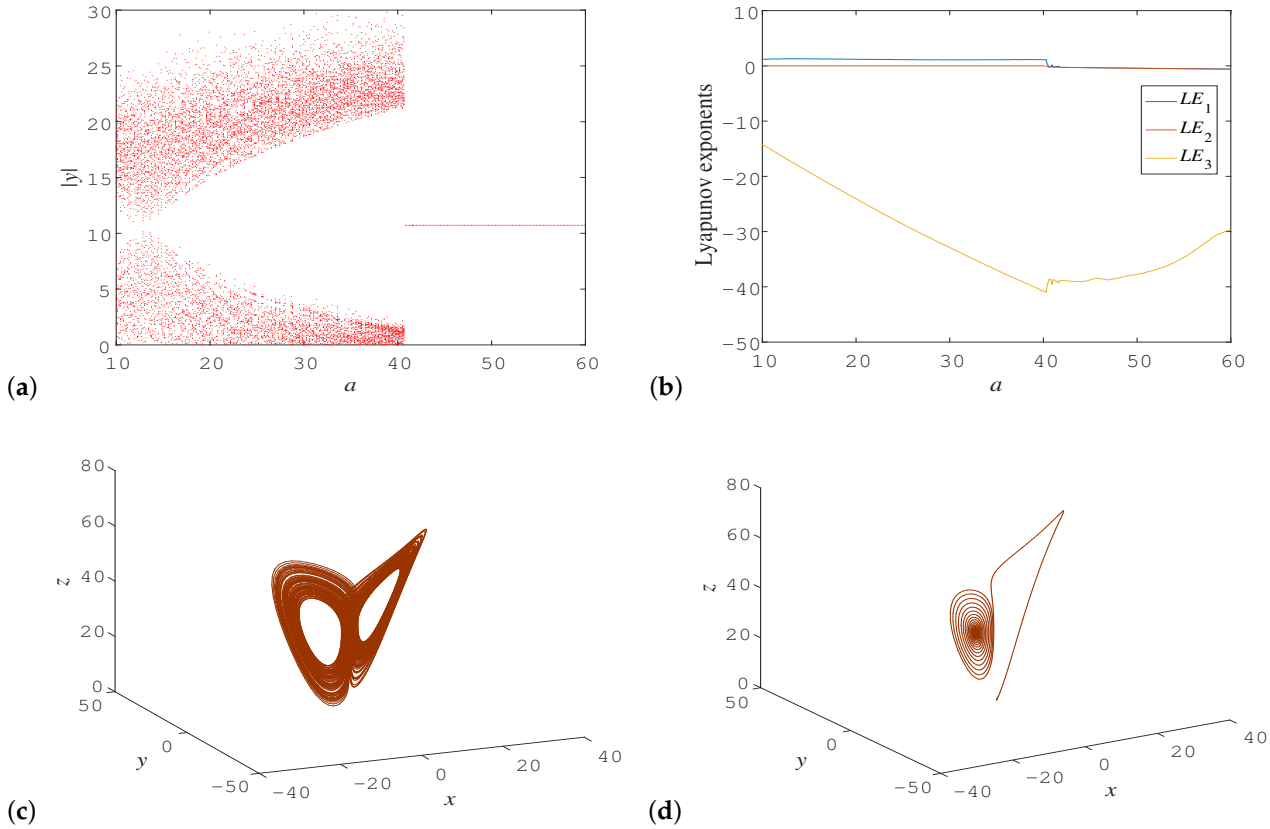

Figure 2. (**a**) Bifurcation diagram and (**b**) Lyapunov exponents spectrum of system (2) vs. a, where $b = 3, c = 35$, and $d = 10$. 3D view of phase portraits with (**c**) $a = 30$ and (**d**) $a = 50$.

Taking the parameter $b \in [0, 5]$, and letting $a = c = 35$ and $d = 10$, the bifurcation diagram and corresponding Lyapunov exponents spectrum are depicted in Figure 3. It is found that the system changes from periodic to chaotic through period-doubling bifurcations, and eventually becomes a stable state, indicating that the system has complicated dynamical characteristics. We note that diverse periodic attractors of the system appear with different parameters b, as shown in Figure 4.

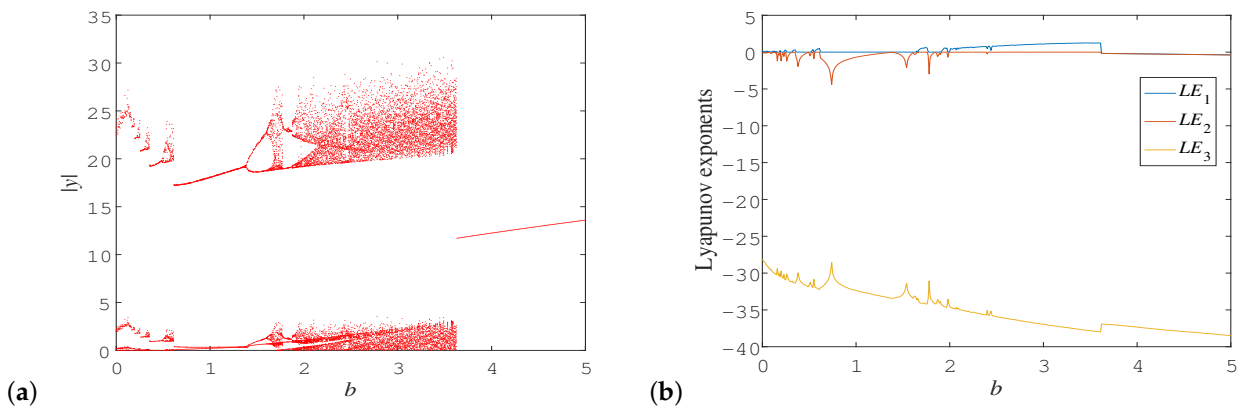

Figure 3. Parameter values $(a, c, d) = (35, 35, 10)$, (**a**) bifurcation diagram, and (**b**) Lyapunov exponents spectrum of system (2) for $b \in [0, 5]$.

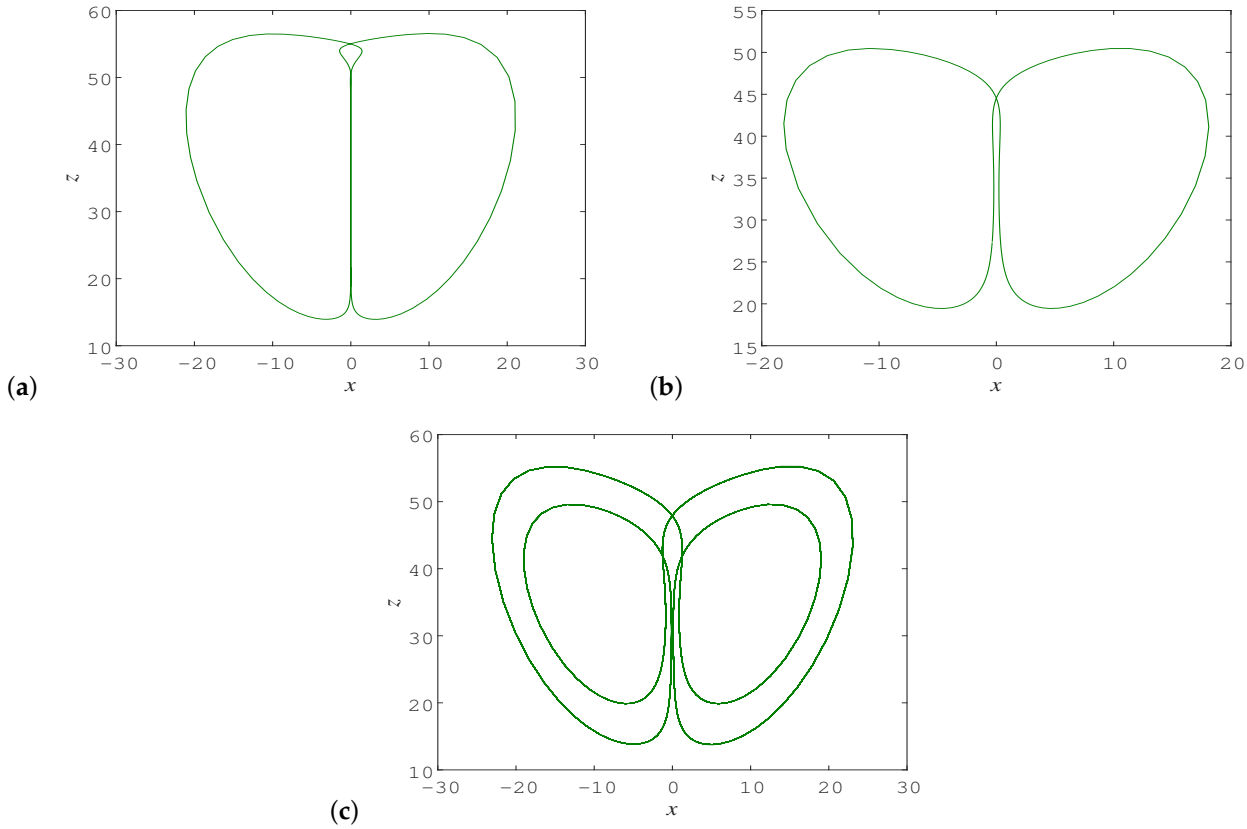

Figure 4. Two-dimensional view of different periodic attractors of system (2), $a = c = 35$ and $d = 10$: (**a**) $b = 0.3$; (**b**) $b = 1$; (**c**) $b = 1.8$.

3.2. Two-Parameter Lyapunov Exponents Analysis

We now explore the global dynamical behaviors by combining two-parameter Lyapunov exponents analysis. To better understand the intricate dynamics, we investigated the effects of two parameters c and d, for which a division diagram can be used to study different kinds of dynamical modes of system (2). Varying c and d within the interval of $c \in [0, 80], d \in [-40, 40]$, and the other parameters are unchanged $(a = 35, b = 3)$, a pseudo-colored map on a 100×100 grid of parameters (c, d) was obtained by calculating the largest Lyapunov exponents; the initial conditions are set $(1, 1, 1)$, as shown in Figure 5. It can be observed in the figure that the magnitudes of the largest Lyapunov exponent values change with color. In particular, the red regions represent chaos, orange domains the periodic attractor, and the rest of the domains are related to stable equilibrium states. At the corresponding values of c and d, system (2) has distinct maximum Lyapunov exponents under different conditions, which further demonstrates that the rich dynamics of the proposed system is complex.

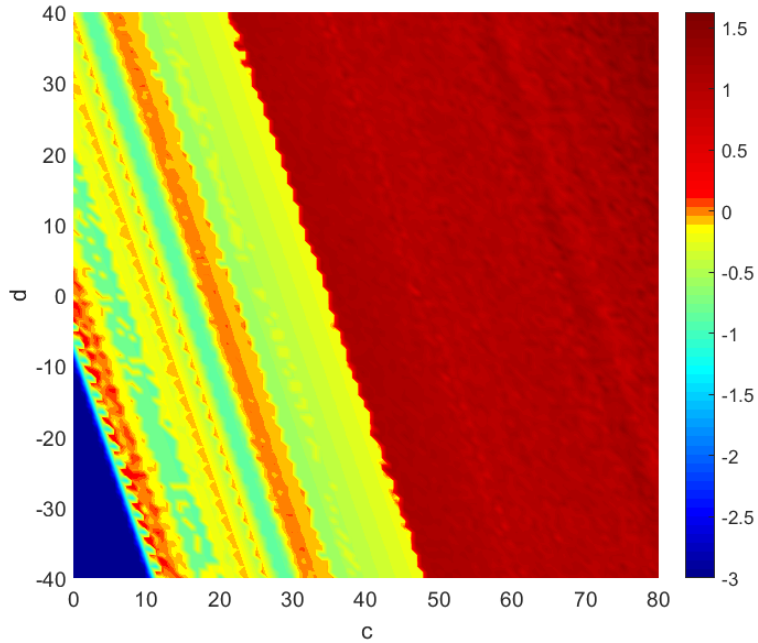

Figure 5. Two-parameter Lyapunov exponents diagram in (c, d) plane with initial values $(1, 1, 1)$.

3.3. Coexisting Attractors and Basins of Attraction

In this subsection, we discuss in detail an investigation into discovering multifarious coexisting attractors in system (2). In the following calculations, we take the parameter values $(a, c, d) = (35, 35, 10)$, and randomly choose various parameters b of the system. As system (2) remains invariant under the transformation $(x, y, z) \to (-x, -y, z)$, which means that any projection of the attractor has rotational symmetry about the z axis, consequently the proposed system may exhibit various coexisting attractors.

First, we explored the coexisting hidden chaotic attractor and stable equilibrium attractors of system (2); the 3D phase portraits are displayed in Figure 6a. Taking the parameters $(a, b, c, d) = (35, 3, 35, 10)$, for initial conditions $(x_0, y_0, z_0) = (1, 1, 1)$, a hidden chaotic attractor can be revealed (yellow color). For initial conditions $(x_0, y_0, z_0) = (-8, -8, 35)$, the trajectory of the system in the phase space converges to the stable equilibrium point E_1 (blue color). For initial conditions $(x_0, y_0, z_0) = (8, 8, 35)$, asymptotically converging behaviors toward another stable equilibrium point E_2 (red color) result.

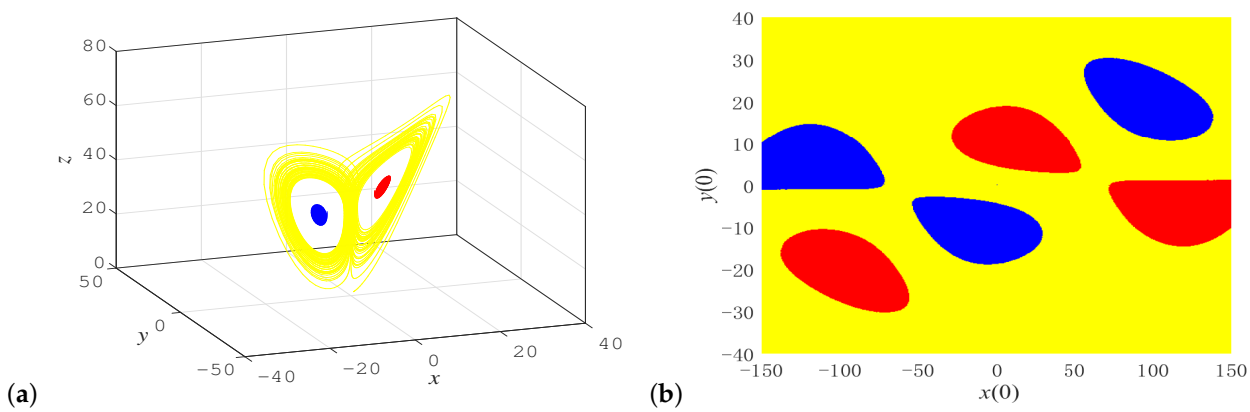

Figure 6. Coexisting hidden chaotic attractor and stable equilibrium state attractors of system (2); $(a, b, c, d) = (35, 3, 35, 10)$: (**a**) 3D phase portraits; (**b**) basins of attraction.

The basin of attraction, which is usually defined as the set of initial points to which the orbits converge for the specified attractor, can exhibit more information about the coexistence of attractions. Thus, the basins of attraction in the $x(0) - y(0)$ plane for

$z(0) = 35$ of the coexisting chaotic attractor and stable equilibrium attractors are displayed in Figure 6b. Three types of basins of attraction are shown in yellow, blue, and red, respectively. Yellow denotes a basin of a chaotic attractor, and blue and red basins represent attractors of two stable node-focus points E_1 and E_2, respectively. It can be observed from Figure 6b that the basins of attraction have the expected symmetry and a smooth boundary. In addition, according to the topological structure of the basin, the attraction basin of the chaotic attractor does not intersect with the small neighborhoods of the stable node-foci E_1 and E_2, which also indicates that the chaotic attractor is hidden.

Moreover, the parameters are set as $(a, b, c, d) = (35, 0.5, 35, 10)$, and two asymmetrical coexisting periodic attractors are illustrated in Figure 7a,b. We also plot the basins of attraction in the $x(0) - y(0)$ plane for $z(0) = 35$ of the two coexisting periodic attractors, as shown in Figure 7c, in which the yellow areas denote the attraction basin of the periodic attractor in Figure 7a and the blue areas the attraction basin of the periodic attractor in Figure 7b. Riddled basins of attraction are observed [42], which illustrates that the state of the system is very sensitive to the initial values. Coexisting periodic attractors of system (2) can also be observed under other parameters, as shown in Figure 8. Taking the parameters $(a, b, c, d) = (35, 0.42, 35, 10)$, there exists in system (2) a green limit cycle for initial values $(-1, -1, 1)$; system (2) also has a limit cycle (shown in purple) for initial values $(1, 1, 1)$. While taking parameters $(a, b, c, d) = (35, 1.5, 35, 10)$, system (2), a limit cycle (shown in blue) exists for initial values $(-1, -1, 1)$, and another limit cycle (shown in red) exists for initial values $(1, 1, 1)$. That system (2) has assorted coexisting periodic attractors proves that rich asymmetric multi-steady states exist in the new system.

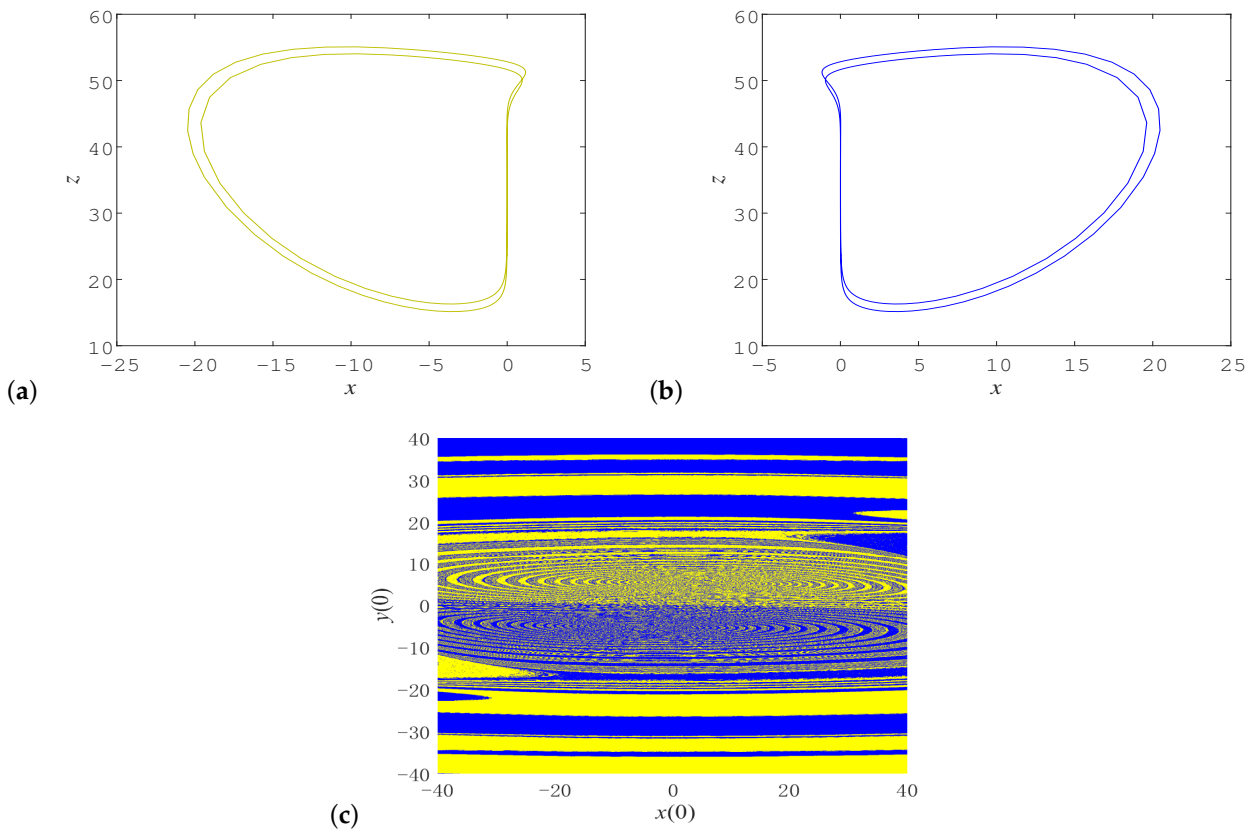

Figure 7. Two coexisting periodic attractors of system (2); $(a, b, c, d) = (35, 0.5, 35, 10)$: (**a**) periodic attractor with initial values $(-1, -1, 1)$; (**b**) another periodic attractor with initial values $(1, 1, 1)$; (**c**) basins of attraction.

Finally, we investigate coexisting chaotic attractors of system (2), and two asymmetrical chaotic attractors are illustrated in Figure 9. Fixing the parameters $(a, b, c, d) = (35, 0.53, 35, 10)$, if we choose initial conditions $(x_0, y_0, z_0) = (-1, -1, 1)$, system (2) has an

asymmetrical chaotic attractor with projection onto the $x - z$ plane depicted in Figure 9a. The other asymmetrical chaotic attractor can also be revealed for initial values $(1, 1, 1)$ due to the symmetry about the z axis [see Figure 9b]; thus, the two chaotic attractors have the same Lyapunov exponents and fractal dimension.

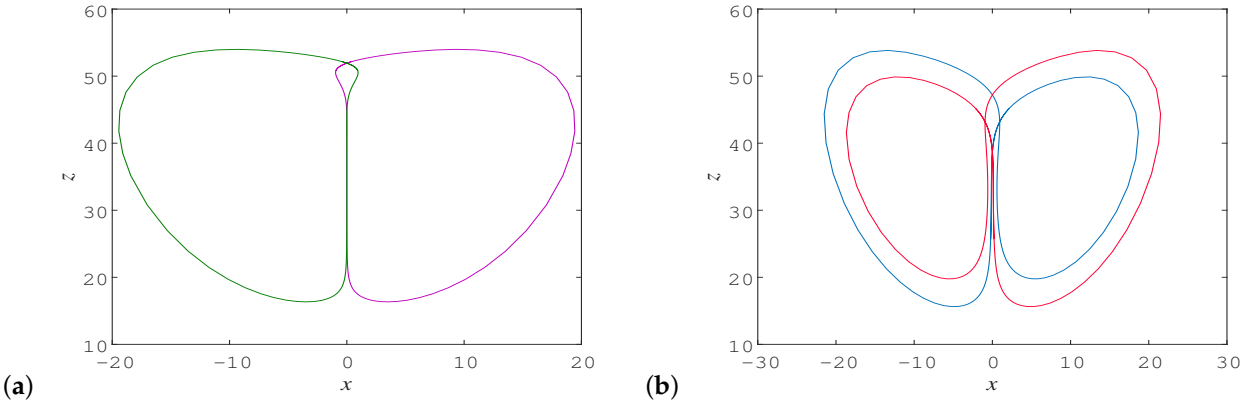

Figure 8. Coexisting periodic attractors of system (2) in (x, z) plane: (**a**) $(a, b, c, d) = (35, 0.42, 35, 10)$ and (**b**) $(a, b, c, d) = (35, 1.5, 35, 10)$.

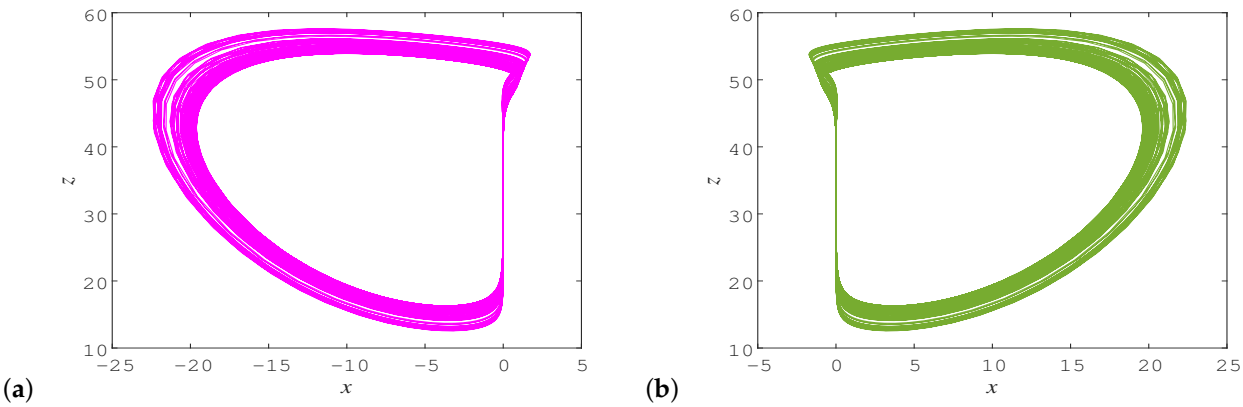

Figure 9. Coexisting chaotic attractors of system (2) in (x, z) plane; $(a, b, c, d) = (35, 0.53, 35, 10)$: (**a**) chaotic attractor with initial values $(-1, -1, 1)$ and (**b**) another chaotic attractor with initial values $(1, 1, 1)$.

3.4. Impact of Constant Term d

We now discuss the impact of the constant term d on the system's stability, including the disappearance of the saddle point at the origin. As the origin $(0, 0, 0)$ is no longer a fixed point when $d \neq 0$, system (2) may possess only two stable equilibria by introducing an additional constant term d. According to the Routh–Hurwitz criterion, it can be seen that the two equilibria are both stable under the conditions $-abc - ad + a^2b + ab^2 + b^2c + bd > 0$ and $2a(bc + d) > 0$. For the parameters $(a, b, c) = (35, 3, 35)$, it yields $-105 < d < 19.6875$. We further found that, when d is negative, system (2) converges to the stable equilibrium point under different initial conditions, and there is no chaotic state. Hence, when we take the parameters $(a, b, c) = (35, 3, 35)$ and $0 < d < 19.6875$, system (2) is able to produce a hidden chaotic attractor. When the parameter $d \geq 19.6875$, the two equilibrium points lose stability and become two saddle-focus points, and the chaotic attractor in system (2) is self-excited.

We also thoroughly examined the impact of the inclusion of the constant term d in the rest of Equation (1) (e.g., dx/dt or dy/dt), which may produce a similar or different impact. When the constant term d is added to the second equation of system (1), the new system no longer has rotational symmetry. By fixing the parameter values $(a, b, c) = (35, 3, 35)$ and changing the control parameter d, we find that three fixed points exist in the system, one of

which is a stable node-focus point and two are saddle-focus points. Regardless of the value of d, the trajectory of the system eventually converges to the stable node-focus point under different initial values, so there is no hidden attractor in the system.

We now investigate the impact when the constant term d is added to the first equation of system (1). Taking the parameters $(a, b, c, d) = (35, 3, 35, 10)$, we found that the system has two stable node-foci coexisting with a chaotic attractor; thus, a hidden attractor also appears in this case. Figure 10 shows the basins of attraction for different initial conditions under current parameter values, in which yellow represents a basin of a chaotic attractor, and blue and red denote basins of stable equilibrium points E_1 and E_2, respectively. It can be seen that riddled basins of attraction arise here and that the basin of attraction no longer has symmetric similarity or a smooth boundary. Furthermore, when the parameter b changes, we also find that other types of coexisting attractors no longer exist. This is because the system has no z-axis rotational symmetry, which is the main difference between it and system (2). Therefore, we conclude that the new system obtained by adding the constant term d to the third equation of Equation (1) has both hidden attractors and coexisting attractors, and that its dynamic behaviors are more complex.

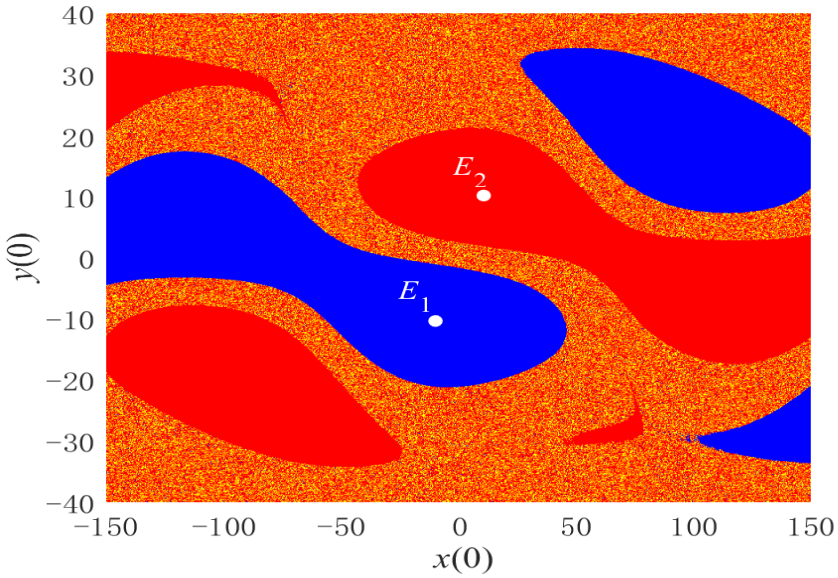

Figure 10. Riddled basins of attraction in $x(0) - y(0)$ initial plane with $z(0) = 35$.

3.5. Offset Boosting Control

Recently, a new category of chaotic systems called variable-boostable systems was proposed. In such a system, the variable can be boosted to any level and switched between a bipolar and unipolar signal, which is convenient for chaotic applications, as it can be used for amplitude control and reducing the number of components required for signal conditioning [43–46]. The state variable y appears twice in system (2), and thus it can be easily controlled. We offset-boost the state variable y by the transformation $y \to y + w$, where w denotes a constant. System (2) can be rewritten accordingly as

$$\begin{aligned} \frac{dx}{dt} &= a(y + w - x), \\ \frac{dy}{dt} &= cx - xz, \\ \frac{dz}{dt} &= x(y + w) - bz - d. \end{aligned} \tag{5}$$

To better illustrate this phenomenon, the offset-boosting of the chaotic attractor is shown in Figure 11 when the control parameter w is altered. The 2D projection of the attractor onto $y - z$ phase space is shown in Figure 11a and the corresponding time-

sequence diagram given in Figure 11b. It can be observed that a bipolar signal is obtained for $w = 0$ (blue), a positive unipolar signal for $w = -35$ (green), and a negative unipolar signal for $w = 35$ (red). Therefore, we can transform the chaotic signal y from bipolarity to unipolarity when varying the control parameter w. Meanwhile, we also calculated the Lyapunov exponents spectrum versus w and found that the three Lyapunov exponents remain invariant, indicating that the state of system (5) does not undergo changes with the offset w.

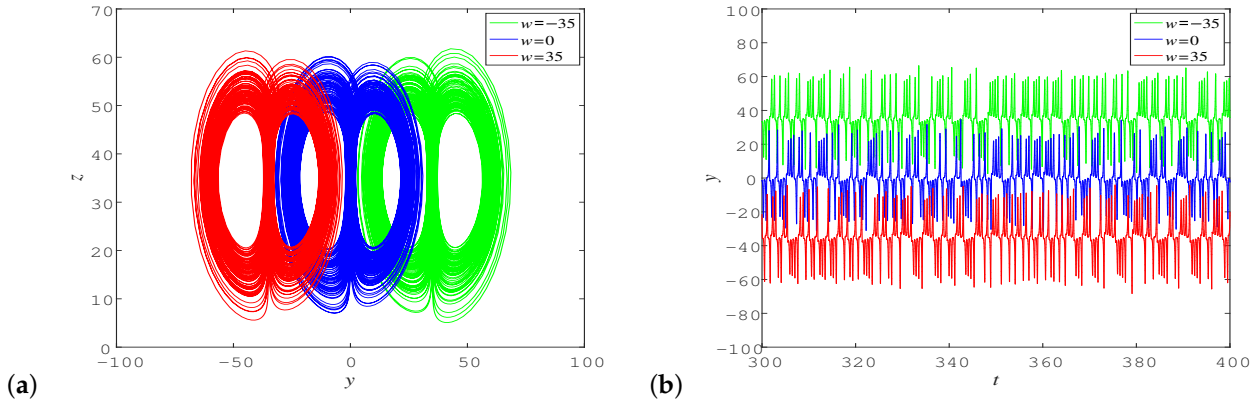

Figure 11. Offset boosting of chaotic attractor when varying control parameter w for $(a, b, c, d) = (35, 3, 35, 10)$: (**a**) in $y - z$ plane and (**b**) state y with different values of the offset boosting controller w. All computed for initial values $(1, 1, 1)$.

Through the above discussion, it is deduced that the new system (2) with a hidden double-wing chaotic attractor has potential chaos-based applications by selecting offset boosting control. In summary, the introduction of the offset w can flexibly shift the position of the chaotic attractor in the y direction in phase space, which has great application value in engineering.

4. One-Dimensional Symbolic Dynamics for Unstable Cycles Embedded in Hidden Chaotic Attractor

To systematically calculate all unstable cycles embedded in the hidden chaotic attractors, we must encode the orbits by means of symbolic dynamics [47]. By selecting an appropriate Poincaré cross-section, the continuous flow can be transformed into a discrete map. Figure 12 shows the first return map of system (2) for $(a, b, c, d) = (35, 3, 35, 10)$. When we choose a special Poincaré section $z = 35$, the initial values are $(1, 1, 1)$, where a dense point with a unimodal structure is presented, which implies that all cycles extracted can be encoded with two letters by 1D symbolic dynamics. Because only one critical point x_c for which $f(x_c)$ reaches the extremum value exists within the interval, a simple division of the phase space is whether a given orbit falls to the left or right of the critical point. If $x_i < x_c$, it is marked as symbol 0; if $x_i > x_c$, then it is marked as symbol 1. In the second iteration, we redefine each partition according to the two-step iteration of the points to obtain four partitions. In this way, we can partition the phase space into different regions, and mark each region with its own unique symbol.

In this work, the variational method [48] was adopted to perform the calculations. Two simplest periodic orbits, marked with symbols 0 and 1 (see Figure 13), can be considered as basic building blocks with which to construct the initial loop guess of more complex periodic orbits. Through 1D symbolic dynamics, we constructed the initial loop guess corresponding to each symbol sequence within the topological length of 5, and calculated the real periodic orbits. Their symbol sequences, periods, and coordinates of a point on the periodic orbits are tabulated in Table 3, from which the symmetry of the system can also be reflected. We also draw the cycles with different topological lengths in 3D phase space in Figure 14.

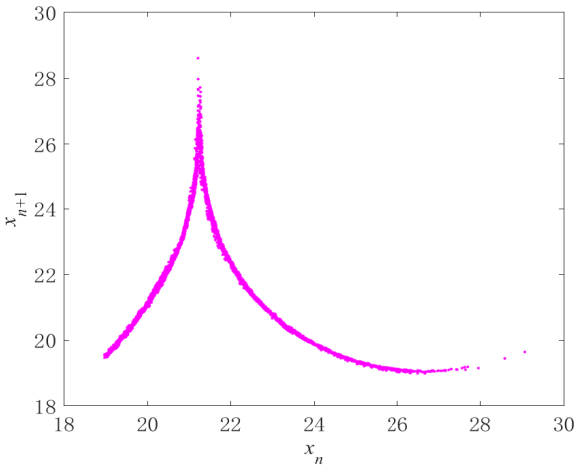

Figure 12. First return map of system (2) under parameters $(a, b, c, d) = (35, 3, 35, 10)$; the Poincaré section is taken as $z = 35$.

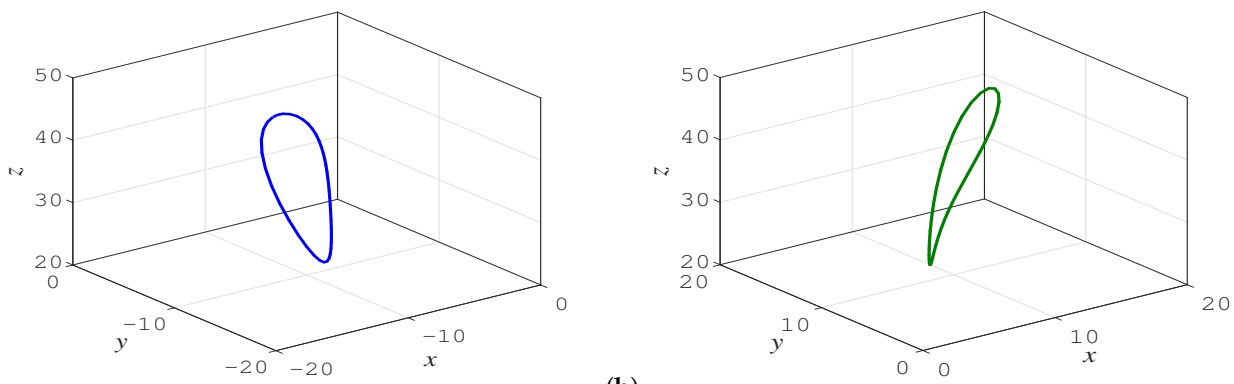

(**a**) (**b**)

Figure 13. Two simplest periodic orbits as basic building blocks in system (2) for parameters $(a, b, c, d) = (35, 3, 35, 10)$: (**a**) cycle 0 and (**b**) cycle 1.

Table 3. Unstable cycles embedded in hidden chaotic attractor of system (2) up to topological length 5 for $(a, b, c, d) = (35, 3, 35, 10)$.

Length	Itineraries	Periods	x	y	z
1	0	0.468918	−10.393417	−7.216587	43.634264
	1	0.468918	10.393417	7.216587	43.634264
2	01	1.190901	−15.856545	−21.285817	21.799902
3	001	1.768396	−1.142202	0.192829	40.538631
	011	1.768396	1.142202	−0.192829	40.538631
4	0001	2.338366	−5.390366	−2.042326	44.498047
	0011	2.364638	8.016602	2.946163	47.893544
	0111	2.338366	5.390366	2.042326	44.498047
5	00001	2.975663	−0.259779	0.021441	36.277845
	00011	2.939762	−2.797000	−3.617918	20.432365
	00101	2.962243	−15.163685	−7.655255	52.919827
	00111	2.939762	2.797000	3.617918	20.432365
	01011	2.962243	15.163685	7.655255	52.919827
	01111	2.975663	0.259779	−0.021441	36.277845

When the parameters of the system change, the first return map of the system will also be altered accordingly, which may no longer be a 1D unimodal map, but have multiple

branches, thus requiring more symbols to encode periodic orbits. In this case, it is more convenient and effective to establish symbolic dynamics based on the topological structure of orbits [49–51], such as the number of rotations between periodic orbits and equilibrium points. Furthermore, continuous deformation of the cycles with the change of parameters can also be explored by the variational method, which can help us judge the parameter values when the number of cycles or stability changes, and thus confirm the corresponding bifurcation phenomenon [52–54].

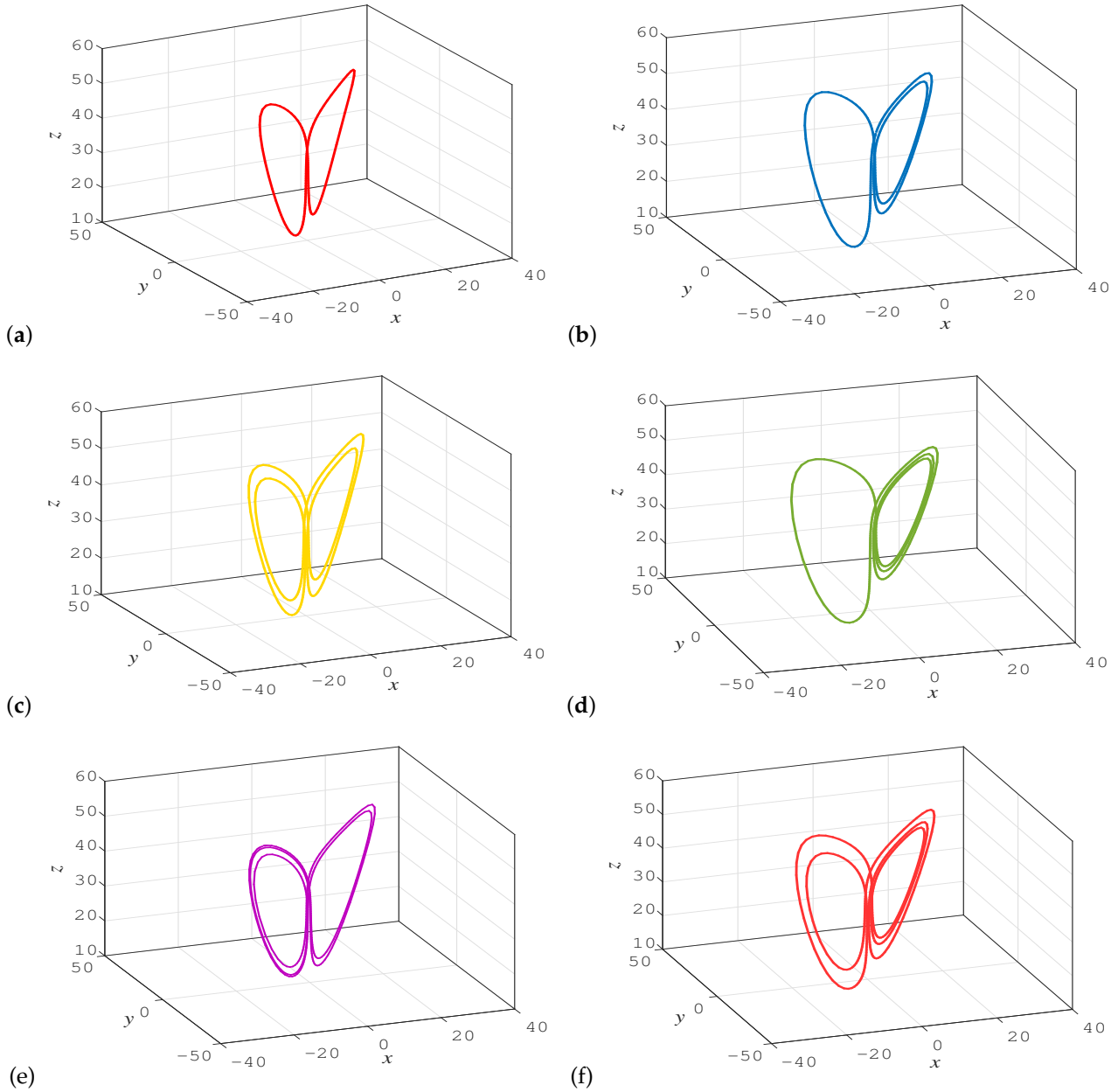

Figure 14. Unstable cycles in system (2) under parameters $(a, b, c, d) = (35, 3, 35, 10)$: Cycles (**a**) 01; (**b**) 011; (**c**) 0011; (**d**) 0111; (e) 00101; (f) 00111.

5. Circuit Implementation

To confirm the engineering feasibility of the new system, we designed an electronic circuit to verify the chaotic behaviors of the mathematical model. In Ref. [55], the circuit realization of a fractional chaotic system regarding capacitors and resistors was proposed to validate the theoretical results obtained via the numerical scheme. Here, the analog circuit of the new double-wing chaotic system (2) was executed in MultiSIM software. The

circuit involves resistors, capacitors, operational amplifiers, and analog multiplier chips. A schematic of a circuit consisting of analog circuit components is illustrated in Figure 15, in which AD811AN units were selected as operational amplifiers. All the multipliers are chosen with an output coefficient of 0.1. When the circuit is executed, we fix the resistors $R_3 = R_9 = R_{16} = 350$ kΩ, input the input signal $-X$ to the resistor R_1, and adjust the value of R_1; the linear dissipative term $-ax$ in the system equation can then be implemented in the circuit. We input the input signal X to the resistor R_7 and adjust the value of R_7; the linear forcing term cx can then be implemented. We adjust the values of $V1$ and R_{15}, implementing the constant term $-d$ in the system equation.

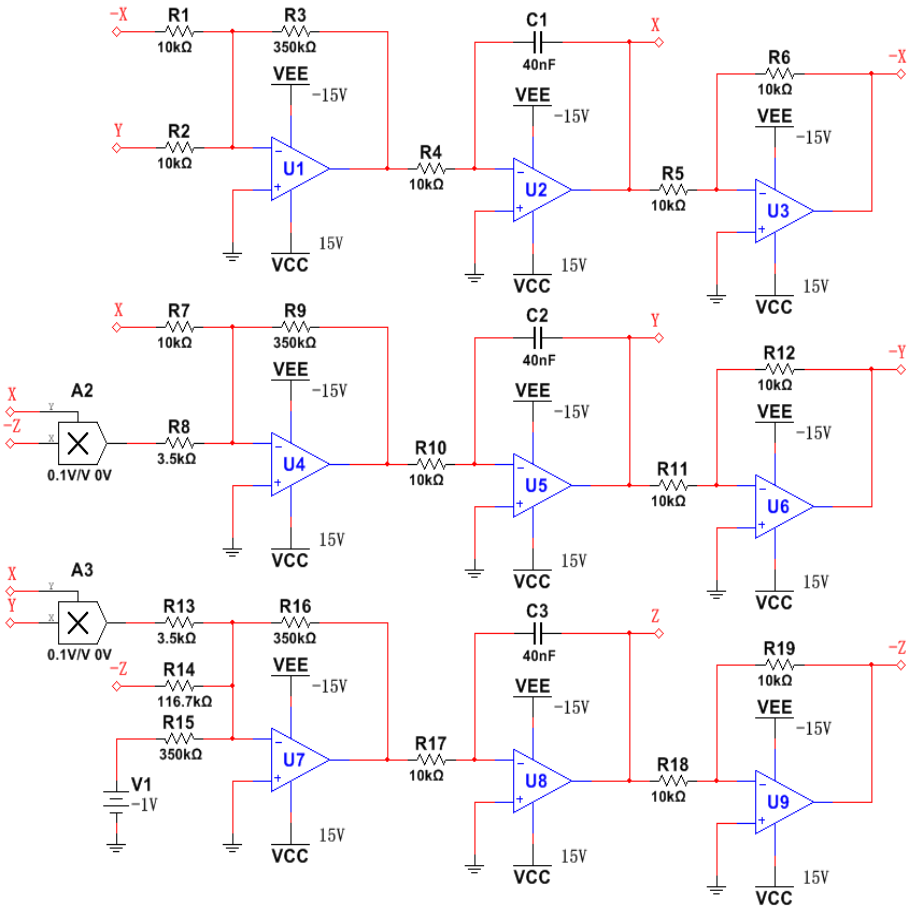

Figure 15. Circuit diagram of system (2).

Because the common power supply voltage is ±15 V, the linear dynamic range of the operational amplifier is ±13.5 V. As can be seen from the simulation results in Figure 1, all the values of state variables (x, y, z) in system (2) are out of the dynamic range, so they require scaling down. The state variables (x, y, z) of system (2) are re-scaled as $X = \frac{1}{10}x$, $Y = \frac{1}{10}y$, and $Z = \frac{1}{10}z$. We set the timescale factor $\tau_0 = \frac{1}{R_0C_0} = 2500$ to better match the system, a new time variable τ is defined instead of t, and $t = \tau_0\tau$. As a result, system (2) after scale transformation is described as

$$\begin{aligned} R_0C_0\dot{X} &= a(Y - X), \\ R_0C_0\dot{Y} &= cX - 10XZ, \\ R_0C_0\dot{Z} &= 10XY - bZ - \frac{d}{10}, \end{aligned} \tag{6}$$

where $a = c = 35$, $b = 3$, and $d = 10$.

By introducing Kirchhoff's circuit laws into the circuit in Figure 15, the relationship between the circuit variables is expressed as

$$\begin{aligned} \dot{X} &= \frac{R_3}{R_2R_4C_1}Y - \frac{R_3}{R_1R_4C_1}X, \\ \dot{Y} &= \frac{R_9}{R_7R_{10}C_2}X - \frac{R_9}{R_8R_{10}C_2}0.1XZ, \\ \dot{Z} &= \frac{R_{16}}{R_{13}R_{17}C_3}0.1XY - \frac{R_{16}}{R_{14}R_{17}C_3}Z + \frac{R_{16}}{R_{15}R_{17}C_3}V_1. \end{aligned} \tag{7}$$

In Equation (7), X, Y, and Z correspond to the voltages on the integrators U2, U5, and U8, respectively, whereas the power supply is ± 15 V. Comparing Equation (6) with Equation (7), we selected $R_{14} = 116.7\,\text{k}\Omega$, $R_8 = R_{13} = 3.5\,\text{k}\Omega$, $R_i = 350\,\text{k}\Omega$ $(i = 3, 9, 15, 16)$, $R_j = 10\,\text{k}\Omega$ $(j = 1, 2, 4, 5, 6, 7, 10, 11, 12, 17, 18, 19)$, $C_1 = C_2 = C_3 = 40$ nF, $V1 = -1$ V.

The oscilloscope outputs showing 2D phase portraits of the circuit simulation are presented in Figure 16, which is very consistent with the numerical results plotted in Figure 1. Thus, the circuit experiment validated the feasibility of the proposed system.

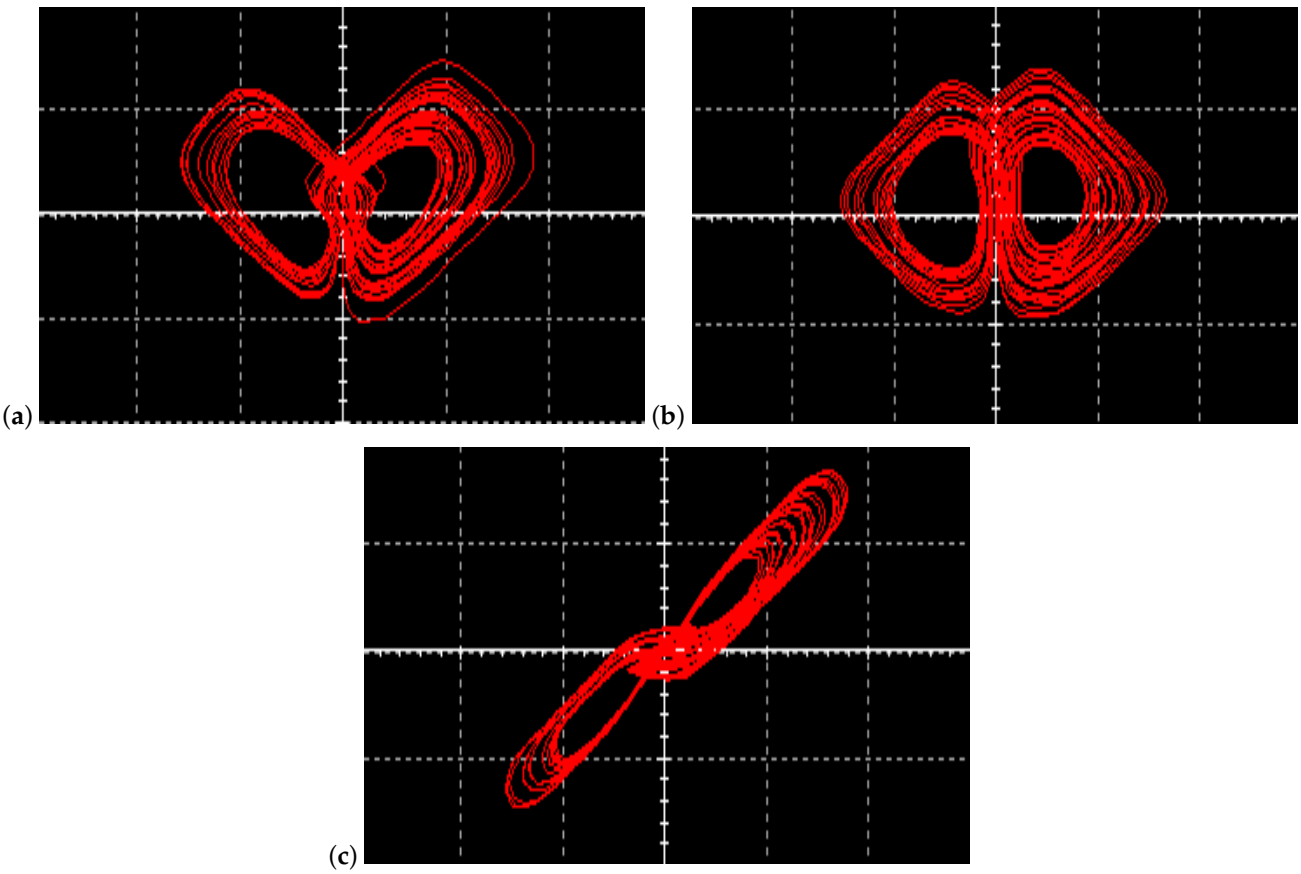

Figure 16. Chaotic behaviors of implemented electronic circuit with initial conditions $(X(0), Y(0), Z(0)) = (1V, 1V, 1V)$ in (**a**) $X - Z$, (**b**) $Y - Z$, and (**c**) $X - Y$ planes.

6. Adaptive Synchronization of Novel Three-Dimensional Chaotic System

To benefit from the rich dynamic characteristics provided by system (2) in chaos-based secure communication, the synchronization problem must be further explored. Hammouch et al. investigated numerical solutions and the identical synchronization of a variable-order fractional chaotic system [56]. Various synchronization methods have been put forward in the literature, including linear and nonlinear feedback, impulse control, and adaptive control. Among these synchronization schemes, adaptive control seems to be the most interesting due to its robustness and simple implementation [57,58]. Here, we employ

the adaptive control method to achieve chaotic synchronization of two identical systems with unknown parameters.

The novel 3D system is considered the master system:

$$\begin{aligned} \dot{x_m} &= a(y_m - x_m), \\ \dot{y_m} &= cx_m - x_m z_m, \\ \dot{z_m} &= x_m y_m - bz_m - d, \end{aligned} \tag{8}$$

and the slave system is described as follows:

$$\begin{aligned} \dot{x_s} &= a(y_s - x_s) + u_x, \\ \dot{y_s} &= cx_s - x_s z_s + u_y, \\ \dot{z_s} &= x_s y_s - bz_s - d + u_z, \end{aligned} \tag{9}$$

in which a, b, c, and d are unknown system parameters, and u_x, u_y, and u_z are adaptive controls. We define the synchronization errors as follows:

$$\begin{aligned} e_x &= x_s - x_m, \\ e_y &= y_s - y_m, \\ e_z &= z_s - z_m. \end{aligned} \tag{10}$$

The error dynamics are easily calculated as

$$\begin{aligned} \dot{e_x} &= a(e_y - e_x) + u_x, \\ \dot{e_y} &= ce_x - x_s z_s + x_m z_m + u_y, \\ \dot{e_z} &= x_s y_s - x_m y_m - be_z + u_z. \end{aligned} \tag{11}$$

The designed adaptive controller is

$$\begin{aligned} u_x &= -\hat{a}(t)(e_y - e_x) - k_1 e_x, \\ u_y &= -\hat{c}(t)e_x + x_s z_s - x_m z_m - k_2 e_y, \\ u_z &= -x_s y_s + x_m y_m + \hat{b}(t)e_z - k_3 e_z, \end{aligned} \tag{12}$$

where k_1, k_2, and k_3 are positive gain constants and $\hat{a}(t), \hat{b}(t), \hat{c}(t)$, and $\hat{d}(t)$ are parameter estimates. By substituting the expression of Equation (12) into Equation (11), we have

$$\begin{aligned} \dot{e_x} &= (a - \hat{a}(t))(e_y - e_x) - k_1 e_x, \\ \dot{e_y} &= (c - \hat{c}(t))e_x - k_2 e_y, \\ \dot{e_z} &= (\hat{b}(t) - b)e_z - k_3 e_z. \end{aligned} \tag{13}$$

The dynamic errors described by Equation (13) can be simplified by taking the parameter estimation errors as

$$\begin{aligned} e_a(t) &= a - \hat{a}(t), \\ e_b(t) &= b - \hat{b}(t), \\ e_c(t) &= c - \hat{c}(t), \\ e_d(t) &= d - \hat{d}(t). \end{aligned} \tag{14}$$

It follows that

$$\begin{aligned} \dot{e_a} &= -\dot{\hat{a}}, \\ \dot{e_b} &= -\dot{\hat{b}}, \\ \dot{e_c} &= -\dot{\hat{c}}, \\ \dot{e_d} &= -\dot{\hat{d}}. \end{aligned} \tag{15}$$

Therefore, Equation (13) can be re-expressed as

$$\begin{aligned} \dot{e_x} &= e_a(e_y - e_x) - k_1 e_x, \\ \dot{e_y} &= e_c e_x - k_2 e_y, \\ \dot{e_z} &= -e_b e_z - k_3 e_z. \end{aligned} \tag{16}$$

The synchronization condition can be established based on the Lyapunov criterion of stability. We consider the quadratic Lyapunov function defined by

$$V = \frac{1}{2}(e_x^2 + e_y^2 + e_z^2 + e_a^2 + e_b^2 + e_c^2 + e_d^2).$$

Differentiating V along the trajectories of the system gives

$$\dot{V} = -k_1 e_x^2 - k_2 e_y^2 - k_3 e_z^2 - e_a(\dot{\hat{a}} - e_x(e_y - e_x)) - e_b(\dot{\hat{b}} + e_z^2) - e_c(\dot{\hat{c}} - e_x e_y) - e_d \dot{\hat{d}}. \tag{17}$$

In view of Equation (17), we take the parameter update laws as

$$\begin{aligned} \dot{\hat{a}} &= e_x(e_y - e_x) + k_4 e_a, \\ \dot{\hat{b}} &= -e_z^2 + k_5 e_b, \\ \dot{\hat{c}} &= e_x e_y + k_6 e_c, \\ \dot{\hat{d}} &= k_7 e_d, \end{aligned} \tag{18}$$

where k_4, k_5, k_6, and k_7 are positive gain constants. By substituting Equation (18) into Equation (17), we obtain

$$\dot{V} = -k_1 e_x^2 - k_2 e_y^2 - k_3 e_z^2 - k_4 e_a^2 - k_5 e_b^2 - k_6 e_c^2 - k_7 e_d^2, \tag{19}$$

which is a definite negative Lyapunov function. According to Lyapunov stability theory, all the synchronization errors e_x, e_y, and e_z and parameter estimation errors e_a, e_b, e_c, and e_d globally and exponentially converge to 0 for random initial values over time.

The effectiveness of the proposed scheme is verified by numerical simulation. The master system is defined as in Equation (8) with parameters $(a, b, c, d) = (35, 3, 35, 10)$ to ensure the chaotic behavior. The gain constants are selected as $k_i = 3$ for $i = 1, 2, 3, 4, 5, 6, 7$. The initial values of the master system, slave system, and parameter estimates are taken as

$$(x_m(0), y_m(0), z_m(0)) = (1, 0, -1), (x_s(0), y_s(0), z_s(0)) = (2, -0.5, -2), (\hat{a}(0), \hat{b}(0), \hat{c}(0), \hat{d}(0)) = (3, 1, 0.5, 12). \tag{20}$$

Thus, the initial values of the errors system (16) are $e_x(0) = 1, e_y(0) = -0.5$, and $e_z(0) = -1$. Figure 17 describes the complete synchronization of the respective states of the master and slave systems, and Figure 18 illustrates the time-history of the synchronization errors and parameter estimation errors. It can be seen that all errors asymptotically converge

to zero with time, indicating that the master and slave systems finally show the same dynamical behavior.

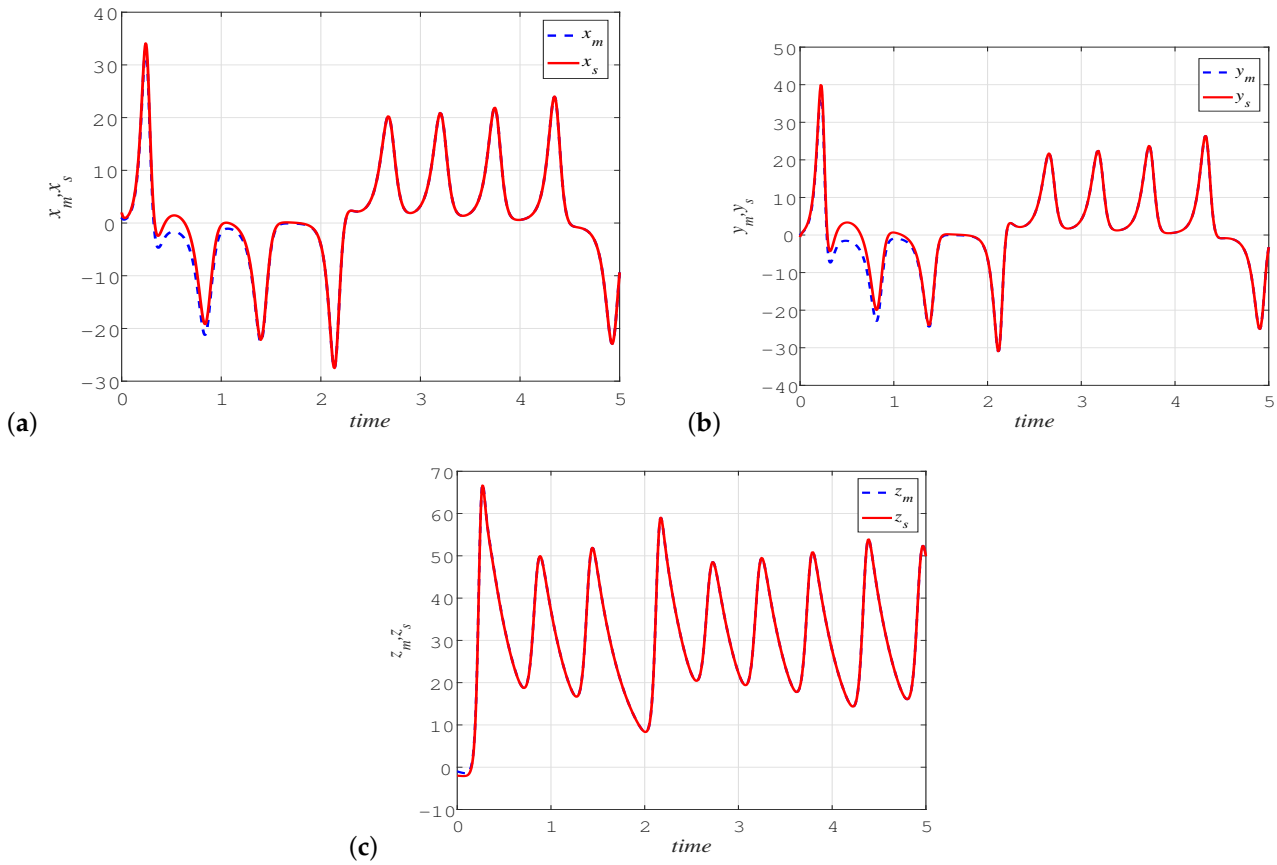

Figure 17. Time evolution sequence diagram of master and slave systems showing results of occurrence of adaptive synchronization. (**a**) x variable; (**b**) y variable; (**c**) z variable.

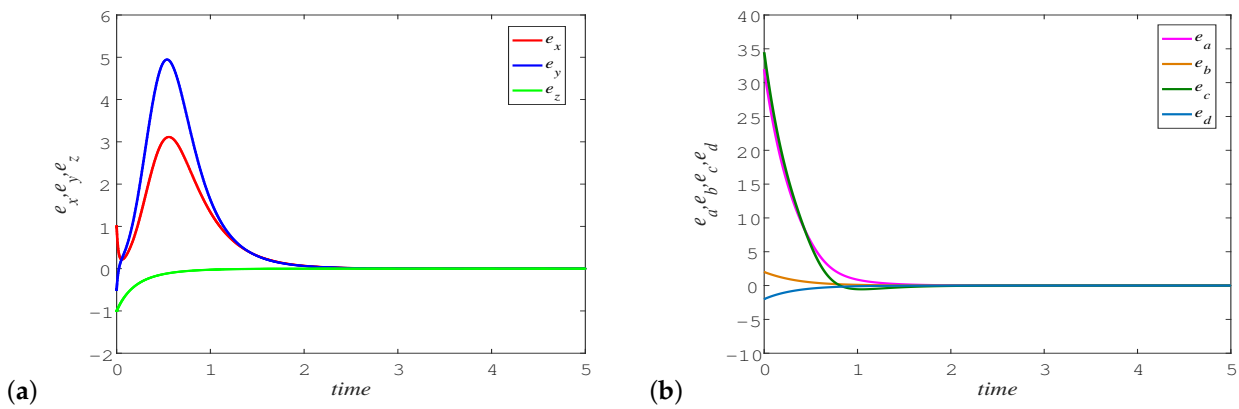

Figure 18. Time evolution of (**a**) synchronization errors e_x, e_y, and e_z, and (**b**) parameter estimation errors e_a, e_b, e_c, and e_d.

7. Conclusions

In this study, a new 3D double-wing chaotic system with two stable equilibrium points was constructed and explored. As the proposed system had only stable equilibria, it was a member of the family of hidden chaotic attractors. Dynamical characteristics, such as bifurcation diagram, basin of attractor, and offset boosting control, were investigated numerically. It was shown that the novel system with hidden attractors had very complex dynamical behaviors. One feature was that various attractors existed in the system, including equilibrium points and periodic and chaotic attractors. The other notable feature was

that the system possessed a variety of different types of coexisting attractors. Unstable cycles embedded in the hidden chaotic attractors were systematically calculated by 1D symbolic dynamics, and circuit simulation for the novel double-wing chaotic system (2) was implemented to demonstrate its flexibility. A scheme for adaptive synchronization of the novel chaotic system with unknown parameters was also investigated. The new hidden attractor chaotic system has potential application prospects in the fields of secure communication, image encryption, and pseudo-random number generators.

As such, how to effectively construct the new system with multi-scroll hidden chaotic attractors is still an open problem; thus, a piecewise-linear or multi-saturated function must be employed to replace continuous functions. The mechanism of generating multi-scroll chaotic attractors is worth exploring. In this respect, the hidden bifurcation routes are considered good candidates. Furthermore, the symmetry of hidden bifurcation routes also warrants further study. The analysis method adopted in this work could promote further research of 3D autonomous chaotic systems and deepen the understanding of both hidden and coexisting attractors.

Funding: This work is supported by the National Natural Science Foundation of China (Grant Nos. 11647085 and 12205257), the Shanxi Province Science Foundation for Youths (Grant No. 201901D211252), and the Scientific and Technological Innovation Programs of Higher Education Institutions in Shanxi (Grant Nos. 2019L0505 and 2019L0554).

Institutional Review Board Statement: Not applicable.

Informed Consent Statement: Not applicable.

Data Availability Statement: The data used to support the findings of this study are available from the corresponding author upon request.

Acknowledgments: I thank the anonymous reviewers for their many insightful comments and suggestions, which substantially improved the manuscript.

Conflicts of Interest: The author declares no conflict of interest.

References

1. Lorenz, E.N. Deterministic nonperiodic flow. *J. Atmos. Sci.* **1963**, *20*, 130–141. [CrossRef]
2. Chua, L.O.; Itoh, M.; Kocarev, L.; Eckert, K. Chaos synchronization in Chua's circuit. *Int. J. Bifurcat. Chaos* **1993**, *3*, 93–108.
3. Sprott, J.C. Some simple chaotic flows. *Phys. Rev. E* **1994**, *50*, 647–650. [CrossRef] [PubMed]
4. Kuate, P.D.K.; Lai, Q.; Fotsin, H. Dynamics, synchronization and electronic implementations of a new Lorenz-like chaotic system with nonhyperbolic equilibria. *Int. J. Bifurcat. Chaos* **2019**, *29*, 1950197. [CrossRef]
5. Negou, A.N.; Kengne, J. Dynamic analysis of a unique jerk system with a smoothly adjustable symmetry and nonlinearity: Reversals of period doubling, offset boosting and coexisting bifurcations. *Int. J. Electron. Commun.* **2018**, *90*, 1–19. [CrossRef]
6. Ma, C.; Mou, J.; Xiong, L.; Banerjee, S.; Liu, T.; Han, X. Dynamical analysis of a new chaotic system: Asymmetric multistability, offset boosting control and circuit realization. *Nonlinear Dyn.* **2021**, *103*, 2867–2880. [CrossRef]
7. Strogatz, S.H. *Nonlinear Dynamics and Chaos: With Applications to Physics, Biology, Chemistry, and Engineering*; Perseus Books: Reading, MA, USA, 1994.
8. Wang, X.; Kuznetsov, N.V.; Chen, G. (Eds.) *Chaotic Systems with Multistability and Hidden Attractors;* Emergence, Complexity and Computation; Springer: Cham, Switzerland, 2021; Volume 40, p. 9.
9. Deng, Q.; Wang, C.; Wu, Y.; Lin, H. Hidden multiwing chaotic attractors with multiple stable equilibrium points. *Circuit World* **2022**, *ahead-of-print*. [CrossRef]
10. Dong, C. Dynamics, periodic orbit analysis, and circuit implementation of a new chaotic system with hidden attractor. *Fractal Fract.* **2022,** *6*, 190. [CrossRef]
11. Yang, Q.; Wei, Z.; Chen, G. An unusual 3d autonomous quadratic chaotic system with two stable node-foci. *Int. J. Bifurcat. Chaos* **2010**, *20*, 1061–1083. [CrossRef]
12. Jafari, S.; Sprott, J.C. Simple chaotic flows with a line equilibrium. *Chaos Soliton. Fract.* **2013**, *57*, 79–84. [CrossRef]
13. Ma, J.; Chen, Z.; Wang, Z.; Zhang, Q. A four-wing hyper-chaotic attractor generated from a 4-D memristive system with a line equilibrium. *Nonlinear Dyn.* **2015**, *81*, 1275–1288. [CrossRef]
14. Kingni, S.T.; Pham, V.T.; Jafari, S.; Woafo, P. A chaotic system with an infinite number of equilibrium points located on a line and on a hyperbola and its fractional-order form. *Chaos Soliton. Fract.* **2017**, *99*, 209–218. [CrossRef]
15. Pham, V.T.; Jafari, S.; Volos, C.; Kapitaniak, T. A gallery of chaotic systems with an infinite number of equilibrium points. *Chaos Soliton. Fract.* **2016**, *93*, 58–63. [CrossRef]

16. Huynh, V.V.; Khalaf, A.J.M.; Alsaedi, A.; Hayat, T.; Abdolmohammadi, H.R. A new memristive chaotic flow with a line of equilibria. *Eur. Phys. J. Spec. Top.* **2019**, *228*, 2339–2349. [CrossRef]
17. Nazarimehr, F.; Sprott, J.C. Investigating chaotic attractor of the simplest chaotic system with a line of equilibria. *Eur. Phys. J. Spec. Top.* **2020**, *229*, 1289–1297. [CrossRef]
18. Vaidyanathan, S.; Pham, V.T.; Volos, C.K. A 5-D hyperchaotic Rikitake dynamo system with hidden attractors. *Eur. Phys. J. Spec. Top.* **2015**, *224*, 1575–1592. [CrossRef]
19. Chowdhury, S.N.; Ghosh, D. Hidden attractors: A new chaotic system without equilibria. *Eur. Phys. J. Spec. Top.* **2020**, *229*, 1299–1308. [CrossRef]
20. Wang, N.; Zhang, G.; Kuznetsov, N.V.; Li, H. Generating grid chaotic sea from system without equilibrium point. *Commun. Nonlinear Sci. Numer. Simul.* **2022**, *107*, 106194. [CrossRef]
21. Dong, C.; Wang, J. Hidden and coexisting attractors in a novel 4D hyperchaotic system with no equilibrium point. *Fractal Fract.* **2022,** *6*, 306. [CrossRef]
22. Almatroud, A.O.; Matouk, A.E.; Mohammed, W.W.; Iqbal, N.; Alshammari, S. Self-excited and hidden chaotic attractors in Matouks's hyperchaotic systems. *Discrete Dyn. Nat. Soc.* **2022** , *2022*, 6458027. [CrossRef]
23. Yan, H.; Jiang, J.; Hong, L. The birth of a hidden attractor through boundary crisi. *Int. J. Bifurcat. Chaos* **2022**, *32*, 2230005. [CrossRef]
24. Pham, V.T.; Jafari, S.; Volos, C.; Fortuna, L. Simulation and experimental implementation of a line–equilibrium system without linear term. *Chaos Soliton. Fract.* **2019**, *120*, 213–221. [CrossRef]
25. Tapche, R.W.; Njitacke, Z.T.; Kengne, J.; Pelap, F.B. Complex dynamics of a novel 3D autonomous system without linear terms having line of equilibria: Coexisting bifurcations and circuit design. *Analog Integr. Circ. Sig. Process.* **2020**, *103*, 57–71. [CrossRef]
26. Tan, Q.; Zeng, Y.; Li, Z. A simple inductor-free memristive circuit with three line equilibria. *Nonlinear Dyn.* **2018**, *94*, 1585–1602. [CrossRef]
27. Tian, H.; Wang, Z.; Zhang, H.; Cao, Z.; Zhang, P. Dynamical analysis and fixed-time synchronization of a chaotic system with hidden attractor and a line equilibrium. *Eur. Phys. J. Spec. Top.* **2022**, *231*, 2455–2466. [CrossRef]
28. Zeng, D.; Li, Z.; Ma, M.; Wang, M. Generating self-excited and hidden attractors with complex dynamics in a memristor-based Jerk system. *Indian J. Phys.* **2022**, 1–15. [CrossRef]
29. Zhang, X.; Wang, C. Multiscroll hyperchaotic system with hidden attractors and its circuit implementation. *Int. J. Bifurcat. Chaos* **2019**, *29*, 1950117. [CrossRef]
30. Li, C.; Sprott, J.C. Multistability in the Lorenz system: A broken butterfly. *Int. J. Bifurcat. Chaos* **2014**, *24* , 1450131. [CrossRef]
31. Doubla, I.S.; Ramakrishnan, B.; Tabekoueng, Z.N.; Kengne, J.; Rajagopal, K. Infinitely many coexisting hidden attractors in a new hyperbolic-type memristor-based HNN. *Eur. Phys. J. Spec. Top.* **2022**, *231*, 2371–2385. [CrossRef]
32. Lai, Q.; Wang, Z. Dynamical analysis, FPGA implementation and synchronization for secure communication of new chaotic system with hidden and coexisting attractors. *Mod. Phys. Lett. B* **2022** , *36*, 2150538. [CrossRef]
33. Ahmadi, A.; Rajagopal, K.; Alsaadi, F.E.; Pham, V.T.; Alsaadi, F.E.; Jafari, S. A Novel 5D chaotic system with extreme multi-stability and a line of equilibrium and its engineering applications: Circuit design and FPGA implementation. *Iran. J. Sci. Technol. Trans. Electr. Eng.* **2020**, *44*, 59–67. [CrossRef]
34. Bao, J.; Chen, D. Coexisting hidden attractors in a 4D segmented disc dynamo with one stable equilibrium or a line equilibrium. *Chin. Phys. B* **2017**, *26*, 080201. [CrossRef]
35. Dang, X.Y.; Li, C.B.; Bao, B.C.; Wu, H.G. Complex transient dynamics of hidden attractors in a simple 4D system. *Chin. Phys. B* **2015**, *24*, 050503. [CrossRef]
36. Bayani, A.; Rajagopal, K.; Khalaf, A.J.M.; Jafari, S.; Leutcho, G.D.; Kengne, J. Dynamical analysis of a new multistable chaotic system with hidden attractor: Antimonotonicity, coexisting multiple attractors, and offset boosting. *Phys. Lett. A* **2019**, *383*, 1450–1456. [CrossRef]
37. Wen, J.; Feng, Y.; Tao, X.; Cao, Y. Dynamical analysis of a new chaotic system: Hidden attractor, coexisting-attractors, offset boosting, and DSP realization. *IEEE Access* **2021**, *9* , 167920–167927. [CrossRef]
38. Pham, V.T.; Volos, C.; Jafari, S.; Kapitaniak, T. Coexistence of hidden chaotic attractors in a novel no-equilibrium system. *Nonlinear Dyn.* **2017**, *87*, 2001–2010. [CrossRef]
39. Yang, Q.; Chen, G. A chaotic system with one saddle and two stable node-foci. *Int. J. Bifurcat. Chaos* **2008**, *18*, 1393–1414. [CrossRef]
40. Wolf, A.; Swift, J.B.; Swinney H.L.; Vastano J.A. Determining Lyapunov exponents from a time series. *Phys. D* **1985**, *16*, 285–317. [CrossRef]
41. Hislop, P.D.; Sigal, I.M. The general theory of spectral stability. In *Introduction to Spectral Theory*; Applied Mathematical Sciences; Springer: New York, NY, USA, 1996; Volume 113.
42. Zhou, L.; You, Z.; Tang, Y. A new chaotic system with nested coexisting multiple attractors and riddled basins. *Chaos Soliton. Fract.* **2021**, *148*, 111057. [CrossRef]
43. Sambas, A.; Vaidyanathan, S.; Zhang, S.; Zeng, Y.; Mohamed, M.A.; Mamat, M. A new double-wing chaotic system with coexisting attractors and line equilibrium: Bifurcation analysis and electronic circuit simulation. *IEEE Access* **2019**, *7*, 115454–115462. [CrossRef]

44. Zhang, Z.; Huang, L.; Liu, J.; Guo, Q.; Du, X. A new method of constructing cyclic symmetric conservative chaotic systems and improved offset boosting control. *Chaos Soliton. Fract.* **2022** , *158*, 112103. [CrossRef]
45. Li, C.; Sprott, J.C.; Liu, Y.; Gu, Z.; Zhang, J. Offset boosting for breeding conditional symmetry. *Int. J. Bifurcat. Chaos* **2018**, *28*, 1850163. [CrossRef]
46. Liu, X.C.; Tu, Q. Coexisting and hidden attractors of memristive chaotic systems with and without equilibria. *Eur. Phys. J. Plus* **2022**, *137*, 516. [CrossRef]
47. Hao, B.L.; Zheng, W.M. *Applied Symbolic Dynamics and Chaos*; World Scientic: Singapore, 1998; pp. 11–13.
48. Lan, Y.; Cvitanović, P. Variational method for finding periodic orbits in a general flow. *Phys. Rev. E* **2004**, *69*, 016217. [CrossRef]
49. Dong, C.; Lan, Y. Organization of spatially periodic solutions of the steady Kuramoto–Sivashinsky equation. *Commun. Nonlinear Sci. Numer. Simul.* **2014**, *19*, 2140–2153. [CrossRef]
50. Dong, C. Topological classification of periodic orbits in the Kuramoto–Sivashinsky equation. *Mod. Phys. Lett. B*, **2018** , *32*, 1850155. [CrossRef]
51. Dong, C. Periodic orbits of diffusionless Lorenz system. *Acta Phys. Sin.* **2018**, *67*, 240501. [CrossRef]
52. Dong, C.; Liu, H.; Li, H. Unstable periodic orbits analysis in the generalized Lorenz–type system. *J. Stat. Mech.* **2020**, *2020*, 073211. [CrossRef]
53. Dong, C.; Jia, L.; Jie, Q.; Li, H. Symbolic encoding of periodic orbits and chaos in the Rucklidge system. *Complexity* **2021**, *2021*, 4465151. [CrossRef]
54. Dong, C.; Liu, H.; Jie, Q.; Li, H. Topological classification of periodic orbits in the generalized Lorenz-type system with diverse symbolic dynamics. *Chaos Soliton. Fract.* **2022**, *154*, 111686. [CrossRef]
55. Sene, N. On the modeling and numerical discretizations of a chaotic system via fractional operators with and without singular kernels. *Math. Sci.* **2022**, 1–21. [CrossRef]
56. Hammouch, Z.; Yavuz, M.; Ödemir, N. Numerical solutions and synchronization of a variable-order fractional chaotic system. *Math. Model. Numer. Simul. Appl.* **2021**, *1*, 11–23. [CrossRef]
57. Gao, X.J.; Cheng, M.F.; Hu, H.P. Adaptive impulsive synchronization of uncertain delayed chaotic system with full unknown parameters via discrete-time drive signals. *Complexity* **2016** , *21*, 43–51. [CrossRef]
58. Azar, A.T.; Volos, C.; Gerodimos, N.A.; Tombras, G.S.; Pham, V.T.; Radwan, A.G.; Vaidyanathan, S.; Ouannas, A.; Munoz-Pacheco, J.M. A novel chaotic system without equilibrium: Dynamics, synchronization, and circuit realization. *Complexity* **2017**, *2017*, 7871467. [CrossRef]